Journal of Nuclear Materials 466 (2015) 634–637

Contents lists available at ScienceDirect

Journal of Nuclear Materials

journal homepage: www.elsevier.com/locate/jnucmat

Xe diffusion and bubble nucleation around edge dislocations in UO_2

Samuel T. Murphy [a, b, *], Paul Fossati [a], Robin W. Grimes [a]

[a] Department of Materials, Imperial College London, Exhibition Road, South Kensington, London SW7 2BP, UK
[b] Department of Physics and Astronomy, University College London, Gower Street, Bloomsbury, London WC1E 6BT, UK

HIGHLIGHTS

- Prediction of enhanced Xe diffusion near edge dislocations in UO_2.
- Identification of an efficient pathway for bubble nucleation and growth.
- Examine how the presence of nano-bubbles influences dislocations in UO_2.

ARTICLE INFO

Article history:
Received 12 May 2015
Received in revised form
16 August 2015
Accepted 4 September 2015
Available online 8 September 2015

Keywords:
UO_2
Xenon
Dislocation
Molecular dynamics

ABSTRACT

Recently it has been suggested that dislocations, generated by radiation damage, may increase the rate of fission gas diffusion from the fuel grains, an affect which is at present not incorporated into fuel performance codes. Therefore, we perform molecular dynamics simulations employing empirical potentials to investigate the diffusion of Xe atoms around edge dislocations in UO_2 to establish the importance of this pathway for fission gas release. The results suggest that for isolated atoms near the dislocation the activation energy for Xe diffusion is dramatically reduced relative to the bulk. However, Xe atoms diffusing along the dislocation cluster together to form small bubbles, these bubbles incorporate all of the isolated mobile Xe atoms thereby inhibiting fast diffusion of Xe along the dislocation core.

1. Introduction

During operation in reactor, uranium and plutonium atoms undergo fission generating a variety of fission products and a largely transient distribution of displaced lattice ions (*i.e.* radiation damage [1,2]). Approximately 26% of fission events result in the production of a krypton or xenon atom. The presence of the noble gas atoms leads to swelling of the fuel which exerts pressure on the cladding thereby increasing the probability of clad failure and release of radioactive material to the coolant [3]. Such release is a significant safety risk and represents the major factor in limiting fuel burn-up in pressurized water reactors (PWR). Therefore, to mitigate this risk it is essential that we develop a comprehensive understanding of the behaviour of fission gasses in nuclear fuels.

Following fission, noble gas atoms will be distributed in the fuel matrix initially accommodated at point defects trap sites, generally thought to be Schottky trivacancy defects [4,5,31]. Diffusion to either bubbles or grain boundaries is then facilitated by associating a further uranium vacancy defect for the gas atom to 'hop' into, with the original vacancy then able to loop around to ensure continued diffusion. The rate determining step in the process is not the migration of the Xe itself but rather the rearrangement of the V_U defect to facilitate net Xe diffusion [6–8]. Activation energies for the overall process depend on the availability of the defect trap sites, which in turn depends on the crystal stoichiometry. For Xe diffusion in UO_{2-x}, UO_2 and UO_{2+x} the activation energies calculated using DFT are 7.04–12.92 eV, 4.15–7.88 eV and 1.38–4.07 eV with the ranges reflecting the way the calculations were performed depending on the charge states of the defects involved and the presence of a Jahn–Teller distortion [7]. Activation energies calculated using empirical pair potentials can vary strongly depending on the choice of potential. Govers et al. examined three different potentials for UO_2 (those of Basak [9], Jackson [10] and Morelon [11]) coupled with different parameterisations for the U–Xe and O–Xe interactions from Geng [12] and Nicoll [13] and recommend values of 6.5 eV, 4.5 eV and 2.4 eV [6] for the different stoichiometric regimes in very good agreement with the experimental values of 6.0 eV, 3.9 eV and 1.7 eV respectively [14].

* Corresponding author. Department of Materials, Imperial College London, Exhibition Road, South Kensington, London SW7 2BP, UK.
E-mail address: samuel.murphy@ucl.ac.uk (S.T. Murphy).

http://dx.doi.org/10.1016/j.jnucmat.2015.09.007

As burn-up is increased there is a marked increase in the dislocation density [15] in the fuel, that is, until the formation of the high burn-up structure [16]. It has been proposed that the relatively lower density of material present in the core of a dislocation may lead to faster diffusion of fission gasses through the fuel grains [17]. Previous simulations have shown that there is a significant enhancement of the diffusivity of the intrinsic O^{2-} and U^{4+} species in the tensile region of edge dislocations' strain fields in UO_2 [18]. It has also been predicted that there is a strong thermodynamic driving force for the segregation of fission products to dislocations [19,20].

The kinetics of Xe diffusion to bubbles along dislocations has been studied using a time dependent finite difference technique and shows that this processes changes non-linearly with the driving force for nucleation in UO_{2+x} [21]. Recent work has challenged the idea that dislocations lead to enhanced diffusion, particularly when charged defects are present [22,23]. The goal of the present work is, therefore, to examine the influence of dislocations on the diffusivity of fission gas atoms, in this case Xe, in UO_2 using molecular dynamics (MD) simulations employing empirical potentials.

2. Methodology

MD simulations were performed using the LAMMPS simulation package [24]. Simulation supercells measuring 280 × 280 × 100 Å and containing four 1/2⟨110⟩{100} dislocations were generated using a 'misfit' approach as described in previous work [18]. The core structure of a dislocation has been shown to have a significant impact on the diffusion of intrinsic species [18]. However, here we have chosen to study just the 1/2⟨110⟩{100} dislocation as this is predicted to have the lowest line energy of the edge dislocations in UO_2 [18,25–27], in agreement with experimental observations of the dominance of the {100} slip plane [28].

Interactions between atoms/ions are represented using a combination of a long range Coulombic component and a short range empirical pair potential. There are a large number of empirical potential models available for UO_2, therefore care must be taken in selecting the most appropriate model. In previous work it was shown that 15 different empirical potential models predict the same ordering for the dislocation stabilities in UO_2 [27]. We adopt one of these, the model of Morelon et al. [11], to allow comparison with previous work. The empirical potentials describing the interaction between Xe and the host UO_2 matrix are taken from Chartier et al. [29] and between Xe atoms is taken from Tang and Toennies [30]. This combination of empirical potential models has been successfully employed previously [29,31].

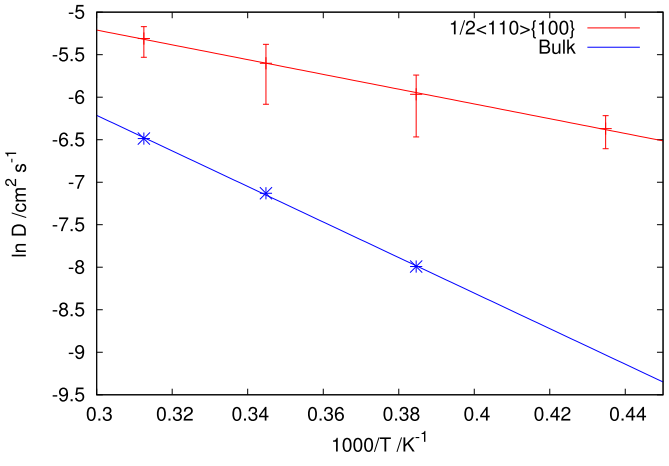

Fig. 1. Arrhenius plot showing the diffusivity of Xe within 20 Å of a 1/2⟨110⟩{100} dislocation compared to in the bulk. The red points correspond to the MSD averaged over all 12 dislocations, and the error bars represent the standard deviation across all of the dislocations. The large error bars arise due the random nature of the initial Xe arrangement relative to the dislocations. The results indicate that the diffusivity of Xe is significantly higher in the vicinity of the dislocation than in the bulk. (For interpretation of the references to colour in this figure legend, the reader is referred to the web version of this article.)

Table 1
Activation energies and diffusion coefficients for Xe diffusion.

System	E_a/eV	D_0/cm s^{-1}
1/2⟨110⟩{100}	1.62	0.0020
Bulk	3.64	0.00035

A concentration of 1.5% Xe was introduced into the simulation supercells by randomly removing U atoms along with two of their O neighbours (thus creating Schottky units) and placing Xe atoms in these trivacancies. While this represents a relatively high Xe concentration it is essential that there is sufficient Xe to sample different regions of the dislocation's strain fields. At the start of the simulation a cylindrical region, of radius 20 Å, centred on each dislocation was defined and all Xe atoms inside these cylinders were identified. The simulation supercells were initially subjected to energy minimisation using a conjugate gradient algorithm, before being equilibrated under constant pressure conditions using the Parrinello–Rahman barostat [32] at a series of temperatures between 2300 and 3200 K for 20 ps with a timestep of 1 fs. These high temperatures were required to ensure that the extent of Xe

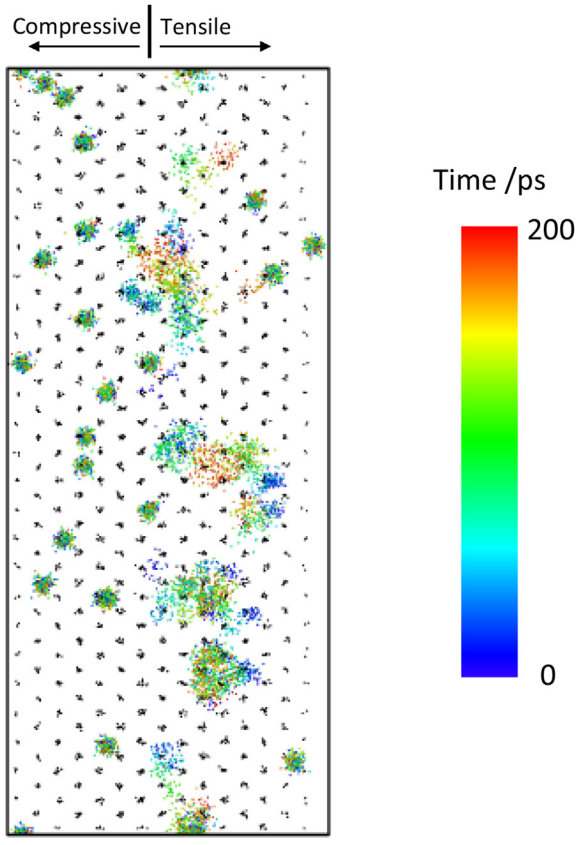

Fig. 2. Superposition showing the positions of Xe atoms surrounding a dislocation. Black spheres correspond to U^{4+} ions and the Xe atoms are coloured according to the simulation time. Xe atoms in the compressive region of the strain field do not diffuse on the timescale of the simulation and so simply oscillate about their initial position. By contrast, Xe atoms in the tensile region are able to diffuse to form small nanoclusters.

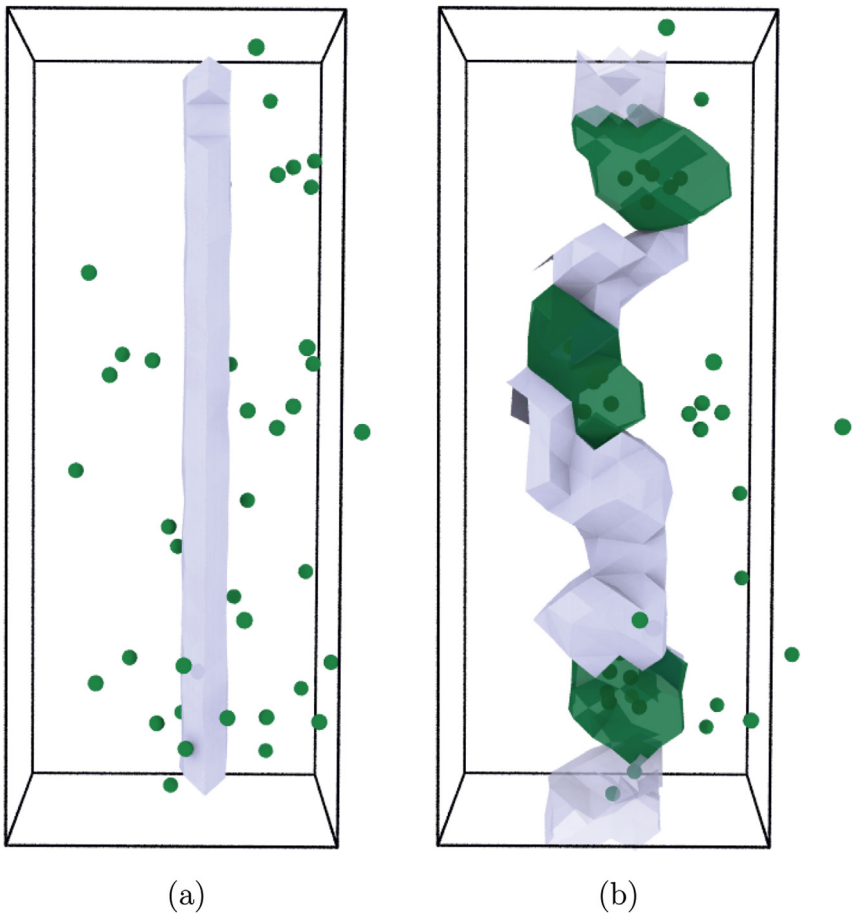

Fig. 3. Snapshot of the Xe atom positions around one of the dislocations: a) initially; b) after 200 ps at 3200 K. The green spheres represent Xe atoms, the green surfaces represent the nano-bubbles and grey surfaces show the position of the dislocation core as detected by the DXA method [36]. Initially, there are 37 clusters; only 19 remain at the end of the simulation. Also visible are the distortions to the initially straight dislocations due to the Xe nano clusters. (For interpretation of the references to colour in this figure legend, the reader is referred to the web version of this article.)

diffusion is statistically significant. The mean-squared displacement (MSD) of Xe atoms, included initially in each of the cylinders, was calculated over a period of 200 ps within the microcanonical (NVE) ensemble (note that Xe atoms leaving/entering the cylinders during the simulation were not excluded/included in the calculation of the MSD). The MSD may then be plotted as a function of time and the diffusivity, D, can be determined following equation (1):

$$D = \lim_{t\to\infty} \frac{1}{2d} \frac{\left[\overrightarrow{r_i}(t) - \overrightarrow{r_i}(t_0)\right]^2}{t} \quad (1)$$

where, d is the dimensionality of the system and t is time. The gradient of the Arrhenius plot of the natural log of the diffusivity against $1/T$ is then E_a/k_B, where E_a is the activation energy, k_B is Boltzmann's constant and the diffusion coefficient can be determined from the intercept with the y-axis.

The small number of Xe atoms close to the dislocations combined with the random nature of their initial positions relative to the dislocation can have a significant influence on their motion and ultimately diffusivities. Therefore, three simulations each with a different starting arrangement of Xe atoms were performed for each temperature.

In order to compare the diffusion of Xe around dislocations and in the bulk crystal, an identical series of simulations as described above was performed where the supercells did not contain the dislocations and the MSDs were calculated for all Xe atoms in the cell. As the number of Xe atoms in the whole supercell is sufficient to ensure the results are statistically significant these simulations were not repeated.

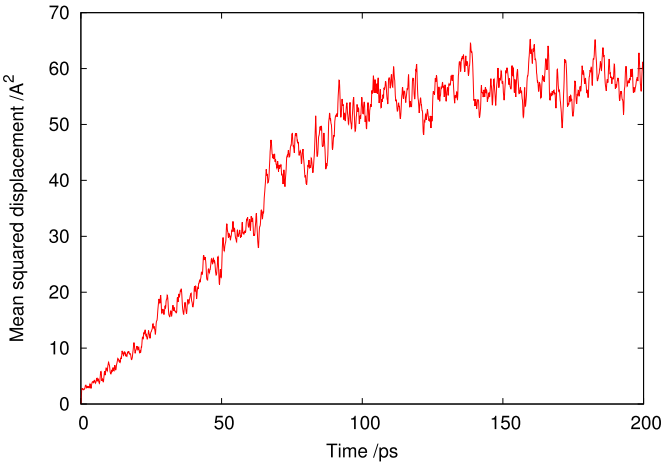

Fig. 4. Example showing the MSD as a function of time around a 1/2⟨110⟩{100} edge dislocation. The MSD initially increases linearly as the Xe atoms diffuse around the dislocation, however, as the atoms forms clusters they become immobile the MSD plateaus.

3. Results

An Arrhenius plot showing the Xe diffusivity within 20 Å of a dislocation compared to the bulk is presented in Fig. 1. The points correspond to the MSD averaged across all of the dislocations and the error bars represent the standard deviation in the MSDs around the 12 different dislocations. It is clear from the plot that Xe diffusivity is significantly increased due to the presence of the dislocations and this effect is more apparent at lower temperatures.

Activation energies and diffusion coefficients for dislocation assisted and bulk diffusion are presented in Table 1. The activation energy for Xe diffusion in the bulk was predicted to be 3.64 eV. Govers et al. [33] present a value of 2.89 eV from their simulations of bulk Xe diffusion in polycrystalline UO_2. We note that as this was a polycrystalline sample the bulk regions may have been subjected to strain, therefore the values may not be directly comparable. As mentioned previously, activation energies calculated using statics techniques such as the nudged elastic band (NEB) [34] with empirical potentials predict Xe activation energies in stoichiometric $UO_2 \approx 4.5$ eV. However, it should be noted that at the temperatures studied here the oxygen sublattice would be mobile and this may aid Xe diffusion [8].

Around the dislocations the activation energy for Xe diffusion is dramatically reduced to 1.62 eV. However, this is still a higher activation energy than for Xe diffusion around grain boundaries in UO_2 (i.e. 0.5 eV [33]). Xe diffusion occurs predominantly in the tensile region of the dislocation strain field, close to the dislocation core where the strain is greatest as shown in Fig. 2. This is because in the tensile part of the strain field the interatomic distances are slightly greater thereby reducing the forces between atoms and hence the energy required to move ions out the way as the Xe atom moves between sites. By contrast Xe atoms in the compressive region of the dislocation strain field are less mobile than in the bulk. A similar observation was made for U^{4+} diffusion in previous work [18].

As the Xe atoms move along the dislocation they encounter other Xe atoms and form small clusters, as has been observed around grain boundaries in UO_2 [33,35]. A strong thermodynamic driving force for cluster nucleation was identified in previous work [31] and this force also acts to prevent resolution from the clusters to the matrix. These observations are consistent with experimental observations that show dislocations are decorated with secondary phase particles and fission gas bubbles [16]. An example of the clustering around a dislocation is presented in Fig. 3.

Xe clusters, once formed, appear to be relatively immobile. Therefore, as the number of Xe atoms incorporated into the clusters increases the number of mobile Xe atoms decreases thereby inhibiting overall Xe diffusion. Fig. 4 shows the MSD as a function of time for Xe diffusing around a $1/2\langle 110\rangle\{100\}$ edge dislocation at 3200 K. Initially the MSD increases linearly due to the diffusion of isolated Xe atoms; however, as the simulation proceeds the Xe atoms form immobile clusters and the MSD plateaus as the number of mobile Xe atoms is reduced. In this particular example all of the mobile Xe atoms have become incorporated into clusters and now diffuse on a time scale greater than that covered by the MD simulations. Consequently, this process should not be thought of as diffusion but rather an irreversible rearrangement of the atoms in the region surrounding the dislocation.

Also evident from Fig. 3 is how the dislocation becomes distorted around the Xe nano clusters. The middle Xe cluster shown in Fig. 3(b) is located adjacent to the dislocation, however, the clusters at the top and the bottom have been absorbed into the core of the dislocation. The dislocations themselves are then pinned to the nano clusters resulting in an increase in the critical shear stress for dislocation glide. Piling up of dislocations on fission gas bubbles has been proposed as one of the mechanisms responsible for the formation of the high burn-up structure [16]. Our results suggest that fission gas bubbles can pin dislocations and this will be discussed in future work.

4. Summary

In summary, the simulations suggest that the activation energy for diffusion of Xe in the tensile region of the dislocation strain field is reduced dramatically so long as the Xe atoms are isolated. Once Xe clusters are formed along the dislocations, they act as traps that greatly impede further diffusion, effectively blocking the dislocation. The activation energy and diffusion coefficients that we have calculated, therefore, should be considered as estimates for the Xe diffusion rate to nano bubble trap sites along dislocations. Thus, in the absence of dislocations Xe atoms move through the lattice in three dimensional space. By contrast, Xe atoms in the vicinity of dislocations are swept-up and channelled along the dislocation to bubbles where they become trapped.

Acknowledgements

All calculations were performed using the Imperial College High Performance Computing Service. STM acknowledges funding from EPSRC (EP/I003320/1) under contract EN20100200. PF acknowledges funding from the Consortium for the Advanced Simulation of Lightwater reactors (CASL) under contract (4000118741).

References

[1] L. Van Brutzel, M. Rarivomanantsoa, J. Nucl. Mater. 358 (2–3) (2006) 209–216.
[2] L. Van Brutzel, M. Rarivomanantsoa, D. Ghaleb, J. Nucl. Mater. 354 (2006) 28.
[3] B. Cox, J. Nucl. Mater. 172 (1990) 249–292.
[4] H.Y. Geng, Y. Chen, Y. Kaneta, M. Kinoshita, Q. Wu, Phys. Rev. B 82 (9) (2010) 094106.
[5] R.W. Grimes, C.R.A. Catlow, Philos. Trans. R. Soc. A 335 (1639) (1991) 609.
[6] K. Govers, S.E. Lemehov, M. Verweft, J. Nucl. Mater. 405 (2010) 252–260.
[7] D.A. Andersson, B.P. Uberuaga, P.V. Nerikar, C. Unal, C.R. Stanek, Phys. Rev. B 84 (2011) 054105.
[8] X.-Y. Liu, B.P. Uberuaga, D.A. Andersson, C.R. Stanek, K.E. Sickafus, Appl. Phys. Lett. 98 (2011) 151902.
[9] C.B. Basak, A.K. Sengupta, H.S. Kamath, J. Alloy. Compd. 360 (2003) 210.
[10] R.A. Jackson, C.R.A. Catlow, J. Nucl. Mater. 127 (1985) 161.
[11] N.D. Morelon, D. Ghaleb, J.M. Delaye, L. Van Brutzel, Philos. Mag. 83 (13) (2003) 1533.
[12] H.Y. Geng, Y. Chen, Y. Kaneta, M. Kinoshita, J. Alloy. Compd. 457 (2008) 465.
[13] S. Nicoll, H. Matzke, C.R.A. Catlow, J. Nucl. Mater. 226 (1995) 51.
[14] W. Miekeley, F.W. Felix, J. Nucl. Mater. 42 (1972) 297–306.
[15] K. Nogita, K. Une, Nucl. Inst. Methods Phys. Res. B-Beam Interact. Mater. At. 91 (1994) 301.
[16] V.V. Rondinella, T. Wiss, Mat. Today 13 (2010) 24.
[17] J. Shea, An Extension to Fission Gas Release Modelling at High Temperatures, EHPG Storefjell, 2013.
[18] S.T. Murphy, E.E. Jay, R.W. Grimes, J. Nucl. Mater. 447 (2014) 143.
[19] P.V. Nerikar, D.C. Parfitt, L.A. Casillas Trujillo, D.A. Andersson, C. Unal, S.B. Sinnott, R.W. Grimes, B.P. Uberuaga, C.R. Stanek, Phys. Rev. B 84 (2011) 174105.
[20] A. Goyal, T. Rudzik, B. Deng, M. Hong, A. Chernatynskiy, S.B. Sinnott, S.R. Phillpot, J. Nucl. Mater. 441 (2013) 96.
[21] P.F. Sui, Z.H. Dai, Sci. China Phys. Mech. Astron. 58 (2015) 052002.
[22] L. Sun, D.M.B. Yildiz, Nat. Commun. 6 (2015) 6294.
[23] D. Marrocchelli, L. Sun, B. Yildiz, J. Amer. Chem. Soc. 137 (2015) 4735–4748.
[24] S. Plimpton, J. Comp. Phys. 117 (1995) 1.
[25] D.C. Parfitt, C.L. Bishop, M.R. Wenman, R.W. Grimes, J. Phys. Condens. Mater. 22 (2010) 175004.
[26] P. Fossati, L. Van Brutzel, B. Devincre, J. Nucl. Mater. 443 (1) (2013) 359–365.
[27] S.T. Murphy, M.J.D. Rushton, R.W. Grimes, Prog. Nucl. Energy 72 (2014) 27.
[28] R.J. Keller, T.E. Mitchell, A.H. Heuer, Acta Metal. 36 (1988) 1073.
[29] A. Chartier, L. Van Brutzel, M. Freyss, Phys. Rev. B 81 (2010) 174111.
[30] K.T. Tang, J.P. Toennies, J. Chem. Phys. 118 (11) (2003) 4976–4983.
[31] S.T. Murphy, A. Chartier, L. Van Brutzel, J.-P. Crocombette, Phys. Rev. B 85 (2012) 144102.
[32] G.J. Martyna, D.J. Tobias, M.L. Klein, J. Chem. Phys. 101 (5) (1994) 4177.
[33] K. Govers, M. Verweft, J. Nucl. Mater. 438 (2013) 134.
[34] G. Henkelman, B.P. Uberuaga, H. Jonsson, J. Chem. Phys. 113 (2000) 9901.
[35] E. Moore, L.R. Corrales, T. Desai, R. Devanathan, J. Nucl. Mater. 419 (2011) 140–144.
[36] A. Stukowski, K. Albe, Modell. Simul. Mater. Sci. Eng. 18 (2010) 025016.